Adv. Elec. Mater. (2020) DOI: 10.1002/aelm.202000803

Charge transfer induced multivalent states with resultant emergent magnetism in transition-metal oxide heterostructures

Wei Niu,[1,8,9] Yue-Wen Fang,[2,3,9] Xiaoqian Zhang,[4] Yakui Weng,[1] Yongda Chen,[4] Hui Zhang,[5] Yulin Gan,[6] Xiao Yuan,[4] Shengjie Zhang,[1] Jiabao Sun,[7] Yile Wang,[1] Lujun Wei,[1] Yongbing Xu,[4,8] Xuefeng Wang,[4,8*] Wenqing Liu[7*] and Yong Pu[1*]

[1]*New Energy Technology Engineering Laboratory of Jiangsu Provence & School of Science, Nanjing University of Posts and Telecommunications, Nanjing 210023, China*
[2]*Laboratory for Materials and Structures, Tokyo Institute of Technology, 4259 Nagatsuta, Midori, Yokohama, 226-8503, Japan*
[3]*NYU-ECNU Institute of Physics, New York University Shanghai, Shanghai 200122, China*
[4]*National Laboratory of Solid State Microstructures, Collaborative Innovation Center of Advanced Microstructures and School of Electronic Science and Engineering, Nanjing University, Nanjing 210023, China*
[5]*Fert Beijing Institute, School of Microelectronics, BDBC, Beihang University, Beijing 100191, China*
[6]*Beijing National Laboratory for Condensed Matter and Institute of Physics, Chinese Academy of Sciences, Beijing 100190, China.*
[7]*Department of Electronic Engineering, Royal Holloway, University of London, Egham, Surrey TW20 0EX, UK*
[8]*Laboratory of Solid State Microstructures, Nanjing University, Nanjing 210093, China.*
[9]*These authors contributed equally*
**Emails: xfwang@nju.edu.cn; Wenqing.Liu@rhul.ac.uk; puyong@njupt.edu.cn*

Abstract:

Transition-metal oxides (TMO) heterostructures provide fertile grounds for creating and manipulating intriguing properties as well as functionalities. At the interface of TMO heterostructures, electronic reconstructions generally occur via charge transfer and lead to an extraordinary spectrum of emergent phenomena but unattainable in their bulk constituents. However, the basic mechanism of charge transfer at the interface is not fully determined or even misunderstood in heterostructures, which may hide the underlying mechanisms and intriguing physics. Herein, an intrinsic charge transfer and resultant exotic ferromagnetism were unambiguously observed in the heterostructures between the nonmagnetic $LaCoO_3$ (LCO) and $SrTiO_3$ (STO). Combining element-specific X-ray absorption spectroscopy and atomic multiplet fitting, we have demonstrated direct evidence of charge transfer-induced multivalence of cobalt ions, interactions of which would contribute to the novel magnetism beyond our intuition, in

concert with first-principles density-functional-theory calculations. Beyond LCO/STO system, we establish a more broadly applicable principle for the heterostructures between 3*d* TMO and STO where charge transfer and resultant multivalence or conducting interfaces are coexistent. Our study represents an advance that the electronic reconstruction and the multiple electron configurations of 3*d* transition metal ions will constitute a powerful tool for the designs of functional materials and creations of unconventional physical properties.

Heterostructures consisting of complex transition-metal oxides (TMO) provide an extraordinary spectrum of possibilities for creating and manipulating emergent phenomena and functionalities, such as complex magnetisms,[1] novel superconductors,[2] tunable spin-charge interconversion[3] and topological states.[4] Among these artificial structures, electronic and structural reconstructions generally occur via charge transfer across the interfaces, yielding plenty of emergent properties but unattainable in the individual bulk constituents.[5-8] Specifically, this transferred charge could interplay with other degrees of freedom in correlated oxides, such as lattice, spin and orbital, thus further tailoring and modifying these intriguing phenomena.

Of late, both theoretical and experimental work has suggested charge transfer, a broadly applicable principle, could tune and control the electronic and spin states in complex oxides heterostructures or superlattices.[9-11] An incipient charge transfer arising from the polar catastrophe processes a high-mobility two-dimension electron gas at the interface of $LaAlO_3/SrTiO_3$ (LAO/STO).[5] Very recently, at the nickelate/iridate interface, a massive electrons were transferred from Ir ions to Ni ions, giving rise to a striking reconstruction and considerably suppressing the strong spin-orbit coupling of 5*d* Ir.[12] For heterostructures exclusively involving 3*d* TMO, interfacial charge transfer-induced magnetism in manganite[13, 14] and ferrite[15] has been proposed in previous studies. However, the basic mechanism of charge transfer at the interface is not fully determined or even misunderstood in heterostructures, which may hide the underlying mechanisms and intriguing physics. For example, the origin of an emergent ferromagnetism has been vigorously investigated but remains controversial in the $LaMnO_3/SrTiO_3$ (LMO/STO) and $LaCoO_3/SrTiO_3$ (LCO/STO) heterostructures.[16-21] Nowadays, it shows that charge transfer-induced multivalent states of Mn have been unambiguously evidenced to induce novel ferromagnetism.[22] Similarly, electronic, spin and orbital similarities among the 3*d* metals may allow this charge transfer-

induced multivalence to be generalized for other TMO heterostructures, while the answer still remains elusive.

Stoichiometric bulk $LaCoO_3$ (LCO) shows a non-magnetic ground state.[23] Interestingly, an emergent ferromagnetism has been observed in their thin films.[20, 24, 25] Mechanisms underlying this exotic ferromagnetic state have been extensively investigated but remain disputable. Most of the studies conclude that the nominal Co^{3+} ions existing in both a low spin state (LS) and a high spin state (HS) under a tensile strain give rise to this ferromagnetism.[20, 26, 27] Besides LS-Co^{3+} and HS-Co^{3+}, bivalent and/or quadrivalent Co ions were also observed.[28, 29] Corresponding exchange interactions between these Co ions with different valence and spin states further contribute to the enhancement or depression of the magnetism. Nevertheless, Co^{2+} and Co^{4+} ions are previously attributed to the unintentional doping, such as oxygen deficiency[28] or cations vacancy.[24, 30] On the other hand, a reliable and comprehensive understanding of this intrinsic multivalence in TMO heterostructures has long been unknown.

In this work, we take the LCO/STO heterostructures as a model to explore the emergent phenomena relevant to the charge transfer. Unexpected ferromagnetism has been observed when the nonmagnetic LCO was epitaxially grown on the STO substrates. By utilizing the X-ray absorption spectroscopy (XAS), atomic multiplet fitting and first-principles calculations, we demonstrate a charge transfer-induced multivalent states of Co ions, including Co^{2+}, LS-Co^{3+}, HS-Co^{3+} and Co^{4+}, coexist in the LCO/STO heterostructures. The ferromagnetism is attributed to the tensile strain-induced spin transition between LS- and HS-Co^{3+} and could be enhanced via the exchange interaction between trivalent and quadrivalent Co ions. Conversely, the accumulation of Co^{2+} at the interface strongly depresses the magnetic properties. Furthermore, beyond LCO/STO heterostructure, we draw a broadly applicable scenario where charge transfer and resultant multivalence or conducting interfaces generally occur in

heterostructures between 3*d* TMO and STO. Our findings deepen the understanding of charge transfer and provide an avenue to tailor emergent phenomena in TMO-based heterostructures.

LCO (001) thin films were epitaxially grown on TiO_2-teminated STO (001) substrates, as schematically illustrated in **Figure 1**a. The *in-situ* reflection high-energy electron diffraction (RHEED) in Figure 1b shows a layer-by-layer film growth with precise thickness control. The deposition process was under the oxygen pressure of 10^{-2} mbar with ozone. Notably, the ozone considerably improves the oxidizability during the deposition, and favors the formation of ferromagnetism, which has been proposed by previous reports.[20] As confirmed by atomic force microscopy (AFM), in Figure 1c, a typical LCO film with 20 unit cells (uc) shows an atomically smooth surface, further indicating the epitaxial growth. Reciprocal space maps (RSM) of a 60-uc LCO sample recorded at the (-1 0 3) diffraction peak of STO substrate in Figure 1d show that both LCO and STO have the same in-plane Q_x value, signifying LCO films are coherently grown on the STO substrate though the thickness is up to 60 uc.[31] Note that since the limit of our facility, the RSM signal is faint for the 20-uc LCO sample but still could tell the coherence, as shown in Figure S1(Supporting Information). In general, all these RSM results indicate the LCO thin films are fully strained on STO substrates with a tensile strain, in good accordance with previous reports.[25]

The predominant novel phenomenon for the heterostructure of LCO/STO is the exotic ferromagnetism since the bulk LCO is otherwise nonmagnetic. The temperature dependence of the magnetic moments with LCO film thickness (t) ranging from 3 uc to 30 uc are shown in Figure 1e. When t > 10 uc, there are clear transitions from nonmagnetic status to ferromagnetic states with the Curie temperature (T_C) of ~ 85 K. Besides, the clear hysteresis loops (Figure S2) further attest the ferromagnetism for the LCO/STO heterostructures. When t is reduced below 10 uc, by contrast, the ferromagnetic transition as well as the T_C is gradually depressed upon decreasing the thickness despite the ferromagnetic characteristic is preserved. Figure 1f summarizes the magnetic moment at T= 10 K (M_{10K}) and T_C as a function of the

LCO thickness. For the samples with t < 6 uc, magnetism is so faint that T_C therefore cannot be exactly derived. Beyond this thickness, the ferromagnetism of the heterostructure develops gradually with the increment of t: T_C is about 40 K (t= 6 uc) and saturates at the value of 85 K (t > 10 uc). Meanwhile, M_{10K} gradually grows with the increasing t and finally reaches a saturation of ~ 0.16 μB/Co (at $\mu_0 H$= 0.1T). This value is comparable to the previous data,[20] but smaller than the theoretical one,[32] providing an information that Co ions with different spin states coexist in LCO.

To reveal the mechanism of the exotic ferromagnetism and the underlying electronic/spin structures of LCO/STO heterostructure, element-specific synchrotron-based X-ray techniques, including soft XAS and X-ray magnetic circular dichroism (XMCD), were applied at the Co and Ti $L_{2,3}$ absorption edges. As illustrated in **Figure 2**a, circularly polarized X-ray was incident at an angle of 60^o with respect to the sample surface, and all spectra were obtained in the total electron yield (TEY) model.[33] Figure 2b depicts these typical XAS spectra at Co-$L_{2,3}$ edges with varied thickness of LCO, besides, validated multiplet calculations of Co^{2+}, Co^{3+} with low-spin state, Co^{3+} with high-spin state and Co^{4+} from Refs. [20] and [34] are served as effective fingerprints of different spin structures and valence states. A few fantastic observations should be noted here. Foremost, the XAS results of these heterojunctions with different LCO thicknesses display prominently different multiplet spectra and comparable to those reference spectra, i.e. multivalent states (Co^{2+}, LS-Co^{3+}, HS-Co^{3+} and Co^{4+}) of Cobalt are simultaneously observed in LCO/STO heterostructures. In particular, the predominant peaks at ~ 780.2 eV for all heterostructures are the characteristics of the LS-Co^{3+}, since the nominal valence of the stoichiometric LCO is trivalent and in a LS ground state. In contrast to the non-magnetic ground state of bulk LCO, novel ferromagnetism has been observed in tensile strained thin film specimens, as pervious reported, thus a spin transition of Co^{3+} ions from a LS to the HS state occurs.[31, 35-37] Herein, our LCO films are fully strained on the STO with a tensile strain, which yields an inhomogeneous mixed-spin states involving LS and HS

states. This is a direct reason why our XAS data could display a hybridized spectrum of HS-Co^{3+} and LS-Co^{3+}, which have been labeled by the second and third dashed line in Figure 2b, respectively. Remarkably, another fingerprint of these multivalent states is the prepeak centered at ~ 777.4 eV, which is the characteristic for the Co^{2+} ions.[36, 38] Previously, Co^{2+} ions are expected to generate due to the introduction of oxygen deficiency.[20, 39] Note that our LCO films were grown under an oxygen rich atmosphere, oxygen vacancies should reduce to the minimum. As a counter check, we also compared the XAS spectra of the as-grown sample and the one fully annealed (600 ^{o}C, 12 hours under fluid oxygen). Both XAS spectra show the prepeak of Co^{2+} (shown in Figure S3). Therefore, the presence of Co^{2+} could not be explained by the oxygen vacancy, and we attribute these divalent ions to the charge transfer as discussed below. Moreover, for all spectra, a pronounced shoulder locates at ~ 781.4 eV, the fingerprint of Co^{4+} ions. To our best knowledge, it is the first time for LCO/STO heterostructures, direct evidence of multivalent Co (Co^{2+}, LS-Co^{3+}, HS-Co^{3+} and especially Co^{4+}) ions is given.

In the light of multivalent states of LCO/STO heterostructures, atomic multiplet fitting were applied to decompose the hybridized XAS spectra. As shown in Figure S4, the best fitted spectra are obtained by a linear combination of Co^{2+}, LS-Co^{3+}, HS-Co^{3+} and Co^{4+} with variant percentages for each heterostructure. These fitting percentages of Co ions with different *t* are summarized and displayed in Figure 2c. The *t*-dependent changes of these percentages indicate the valent states of Co are not uniform in LCO. The intrinsic LS-Co^{3+} dominates the whole sample range, so the content is higher than those of the other valence states all the while. Additionally, the percentage of HS-Co^{3+} is 13.34% when *t*= 4 uc and goes all the way up to 34.54% (*t*= 20 uc). The novel ferromagnetism observed in the LCO/STO heterostructures is more favored with a higher content of HS-Co^{3+}. This is the reason why the ferromagnetism of the heterostructure develops gradually with the increment of *t*, as we discussed above. While the percentage of Co^{2+} is 34.12% at *t*= 4 uc and decreases sharply to 9.24% when *t*= 20 uc. This suggests that Co^{2+} dominates when the LCO films are thin and can

easily accumulate at the interface of LCO/STO (more details could refer to Figure S7). Analogously, the concentration of Co^{4+} presents a similar thickness-dependent decrease from 20.43% to 12.08%. The spin configurations of Co ions contribute to the magnetism and they are determined by the electronic structures. Among the multivalent Co ions, based on the Goodenough-Kanamori-Anderson theory and previous results, magnetic spin states of LCO favor ferromagnetic superexchange between LS-Co^{3+} and HS-Co^{3+} ions.[27, 40] In addition, exchange interaction between Co^{3+} and Co^{4+} could also enhance the magnetism but tetravalent ions at the bare surface are not stable due to the effects of atmospheric exposure.[41] On the contrary, bivalent ions at the interface are always believed to decrease the ferromagnetism and probably lead to a dead layer.[20, 42, 43] This can be further demonstrated in the XMCD spectrum of Co edges, as shown in Figure S5, besides HS-Co^{3+}, LS Co^{3+}, dichroism is also obtained from Co^{4+}. It indicates interactions between Co^{3+} and Co^{4+} lead to the intrinsic ferromagnetism. However, no dichroism is found from Co^{2+}, implying Co^{2+} ions do not contribute to the ferromagnetism. A spin block between these multivalent Co ions also prohibits the hopping process and suppresses the conduction,[21] as experimentally proved in Figure 1g.

XAS measurements on Ti-$L_{2,3}$ edges were also performed for the LCO/STO heterostructures. As displayed in Figure 2d, though the differences in the thickness of LCO films, all spectra, including that of a bare STO substrate as a reference, show the isotropic characteristics, namely a similar electronic structure. For the heterointerfaces such as LAO/STO[20, 44] and $LaTiO_3/SrTiO_3$[45], electrons are transferred to the STO site thus forming a Ti^{3+} state from the Ti^{4+}, the energy difference between these two peaks changes in sharp contrast to the result herein. In addition, all spectra are the same with the one of STO substrate reference. It proves the valence state of Ti remains tetravalent and no Ti^{3+} signal is observed. A possible magnetism from the Ti site can also be ruled out,[46, 47] which is further corroborated by our XMCD results in Figure S5. We now have a picture that all Ti ions keep

the quadrivalence state, and therefore no charge is transferred to STO and electron reconstruction would occur on the other sites, such as LCO.

Charge transfer is generally observed among TMO heterostructures, a prototype is the polar/nonpolar interface of LAO/STO with a polar discontinuity, processing a two-dimensional electron gas.[5] Analogously, (001)-oriented LCO is polar, stacked by alternating layers of $(LaO)^{+1}$ and $(CoO_2)^{-1}$, whereas STO can be separated by $(SrO)^0$ and $(TiO_2)^0$, nonpolar planes. Therefore, interfacial charge transfer is derived to counteract the polar catastrophe at the interface of LCO/STO. In the LAO/STO system, the transferred electrons span both LAO and STO: from the top surface of LAO to the interfacial STO inside since the top of LAO valence band (VB) is larger than the bottom of STO conduction band (CB) and thus the valence state of Ti is reduced from quadrivalent to trivalent.[48] Strikingly, in the case of LCO/STO as schematically shown in Figure S6, considering the valence band offset (E_{VBO}), the top of LCO CB is always lower than the bottom of STO CB (the band gap, E_g, of LCO is 0.6 eV[49]), despite the VB rises upon increasing the *t* of LCO due to the polarity. Beyond a critical thickness, the top of LCO VB is higher than the bottom of LCO CB but still lower than that of STO, under this circumstance, electrons only reconstruct on the LCO site rather than STO. In this vein, electrons are confined within LCO and intrinsically transferred from the surface to the interface of LCO itself, therefore forming Co^{2+} ions dominating at the interface. This scenario echoes the previous experimental demonstration of Co^{2+} ions at the interface whereas no detected Ti^{3+} ions. Due to the electric neutrality of films and the charge conservation, partial surficial Co^{3+} ions turn into Co^{4+} states after transferring electrons to the interface. Correspondingly, multivalence states of LCO/STO heterostructures are the result of the electron reconstruction due to the charge transfer.

To elucidate the charge transfer from first-principles theory, we used density functional theory (DFT) calculations to study the electrostatic potential energy profiles of LCO/STO heterostructures. Structures and potential energy profiles U_E for $(LCO)_2/(STO)_4$ and

$(LCO)_2/(STO)_4$ are shown in **Figure 3**. As expected, the alternatively arranged polar stacks of the charged atomic layers along the *c*-axis give rise to internal electric fields across the LCO layers which are indicated by the silver lines. Since the difference of U_E from the interface to the LCO surface is negative, the electric potential from the interface to the surface is positive, corresponding to an intrinsic electric field pointing to the *c*-axis. A system with such an intrinsic electric field across the overlayers has an infinite surface energy and is not stable[50], the reconstruction of electronic structure is expected to compensate the electric potential and stabilize the system. In our case, the electrons are required to accumulate at the interface to partially screen the internal electric field.

We note that the slope of the macroscopic-averaged potential energy in $(LCO)_2/(STO)_4$ is larger than $(LCO)_4/(STO)_4$ in analogy with LMO/STO[18] and LAO/STO[51] heterostructures, this is because the transferred charge in thicker heterostructures can partially balance the intrinsic electric field[13]. The internal electric field estimated from the average slope of $(LCO)_2/(STO)_4$ and $(LCO)_4/(STO)_4$ is on the order of 0.14 V/Å. This internal electric field is comparable to the LMO/STO heterostructures of 0.177 V/Å[18] and is smaller than the LAO/STO heterostructures of 0.24 V/Å[51]. Considering the strength of the intrinsic electric field of 0.14 V/Å, the electron reconstruction will be initiated when the built-in potential in the LCO layers above an estimated critical thickness of 4.3 Å (~ 1 uc) is larger than the band gap of LCO, and the electrons can only be transferred to the interface LCO layers due to the small E_g of ~0.6 eV and the E_{VBO} of around 1.7 eV (the estimation of E_{VBO} is available in the Supplementary information).

The electron transfer within the LCO overlayers makes the interface layers of LCO electron doped and the surface regions hole doped, which can be expected to induce the original Co^{3+} towards Co^{4+} at the surface and Co^{2+} at the interface, respectively, observed in our experiment. This phenomenon is very likely to have the electronic phase separation that has been observed in bulk manganites[52] and LAO/STO[53], and very possibly in the case of

LMO/STO[22]. Hence, we draw a qualitative picture, as illustrated in **Figure 4**a, besides LS-Co^{3+} and HS-Co^{3+} ions distribute throughout the whole sample, Co^{2+} ions are dominating at the interface while Co^{4+} ions are dominating at the surface.

Beyond the LCO/STO systems, we could go one step further and expand the system to the STO-based 3*d* TMO heterostructures of La*B*O_3/STO (*B* site are the 3*d* transition-metal ions with partially occupied *d* shell[54], unless otherwise specified, *B* = Ti, V, Cr, Mn, Fe, Co, Ni and Cu) for investigating the charge transfer. Previously, for 3*d* TMO, electronegativity differences (also known as electron affinity[9]) determine the magnitude of the charge transfer. As schematically shown in Figure 4b, electronegativity differences decrease as the atomic number increases among the 3*d* transition metal series. For the 3*d* TMO heterostructures and superlattices, electrons should generally transfer from a higher *d* states energy levels of *B* ions to the lower one in principle. Nevertheless, the mechanism of electronegativity difference here is invalid. For example, for La*B*O3/STO heterostructures, *d* states of *B* (except Ti) ions are lower than those of Ti ions from STO, though an electronegativity difference between Ti of STO and *B d* levels exists, no charge would transfer from Ti to *B* ions. An alternative general scenario has been proposed here based on E_{VBO} and E_g in La*B*O_3/STO heterostructures.

All the studied La*B*O_3 in our work are polar and a polar field is developed along the stacking direction,[9] polarity difference at the interface is a primary drive for the charge transfer, thus the cations intermixing and redox reactions[55] are not taken into consideration. As previous theoretical and experimental work proved, the potential difference between the surface and interface of La*B*O_3 is proportional to its thickness.[9] Once the accumulated potential difference is larger than the bottom of the CB of either STO or La*B*O_3, electrons will transfer to compensate the polar discontinuity. Consequently, as shown in the red dashed area of Figure 4c, the top of La*B*O_3 VB turns to be higher than the bottom of STO CB when the thickness is beyond the threshold, considering the E_{VBO}, electrons are transferred from *B* site

to the CB of STO in the vicinity of the interface. This is the reason why conducting interfaces were experimentally observed in the heterostructures of $LaTiO_3$/STO,[45], $LaVO_3$/STO[56], and theoretically demonstrated $LaCrO_3$/STO,[57] and $LaFeO_3$/STO[58] heterostructures. On the other hand, in the blue counterpart of Figure 4c, due to the small E_{VBO} or E_g (i.e. in the cases of *B*= Mn and Co), the top of La*B*O_3 VB is lower than the bottom CB of STO but higher than bottom CB of La*B*O_3, i.e. $E_{g\_LaBO3} < (E_{g\_STO} - E_{VBO})$. When growing the thickness, electrons tunnel from the surface to the interface of La*B*O_3 and emerge in its CB rather than those of STO. As a result, B^{2+} ions dominate at the interface in La*B*O_3 site, whereas B^{4+} ions distribute at the surface mostly, as presented in Figure 4a. This intrinsic charge transfer confined in La*B*O_3 and resultant multivalence states of 3*d* metal ions have been experimentally demonstrated in the LMO/STO,[13, 18] and the current investigated system of LCO/STO. The exchange couplings among these multivalent *d* ions could determine the exotic magnetism in the heterostructures. Note that the *d* states of Ni and Cu hybridize with oxygen *p* states showing metallic behaviors and beyond the scope of current discussion.[59] We further verify this general scheme of charge transfer in La*B*O_3/STO heterostructures theoretically, electronic reconstruction via intrinsic electric fields and E_{VBO} are available in the Supporting information.

In conclusion, we have established the direct evidence of the multivalent states of Co^{2+}, Co^{3+} and Co^{4+} ions due to the charge transfer and a resultant emergent magnetism in LCO/STO heterostructures. Beyond the single heterostructure of LCO/STO, our results established a general charge transfer scenario in heterostructures between 3*d* TMO and STO. Based on the electronegativity difference, bandgap and band offset, charges transfer from La*B*O_3 to STO when *B*= Ti, V, Cr and Fe, whereas electrons only intrinsically transfer within La*B*O_3 from its surface to the interface and lead to the multivalence states when *B*= Mn and Co. Our results broaden the understanding of charge transfer induced emergent phenomena in TMO heterostructures.

Experimental Section

Sample synthesis and characterization: The LCO films were grown by pulsed laser deposition technique on pre-treated TiO_2-terminted STO substrates as described elsewhere.[22] The growth thickness and dynamics were monitored via the RHEED oscillations and patterns. For the high-quality LCO, the optimal growth temperature and oxygen pressure are kept at 600 ºC and 1×10^{-2} mbar with ozone, respectively. It should be noted that the optimal deposition temperature is lower than other TMO and the temperature window for high quality cobaltates is very small by our PLD facility.

Magnetic Measurements: Magnetic measurements were performed via SQUID (Quantum Design) system. The applied magnetic field was in-plane parallel to the (100) orientation of STO. For temperature dependence of measurements, all samples were cooled down to 10 K under the applied magnetic field of 1 T, then measured under 0.1 T in the warm-up process.

X-Ray Absorption Measurements: synchrotron radiation measurements were performed on Beamline I10 at the Diamond Light Source. 100% circularly polarized X-rays were incident at an angle of 60º with respect to the sample surface. The applied magnetic field was 3 T and parallel to the X-rays. All spectra were obtained at 10 K in TEY model.

First-Principles Calculation: All the spin polarized DFT calculations with the Vienna Ab-initio Simulation Package (VASP) were performed[60, 61]. The revised version of Perdew-Burke-Ernzerhof generalized gradient approximation for solids (PBEsol)[62] was used as the exchange correlation functional. Spin polarized version of the exchange functional was used with the inclusion of Hubbard *U* for on-site electronic Coulomb interactions of 3*d* orbitals. More details can be found in Supplementary information.

Acknowledgements
W. Niu and Y.-W. Fang contributed equally to this work. This work was supported by the National Key Research and Development Program of China (Grant No. 2017YFA0206304), the Natural Science Foundation of China (Grant Nos: 11874203, 61822403, U1732159, 61874154, 61874060, 11904174, 11804168), Jiangsu Specially-Appointed Professor program, Natural Science Foundation of Jiangsu Province (Grant Nos. BK20181388, BK20190729, BK20180736), Oversea Researcher Innovation Program of Nanjing, NUPTSF (Grant Nos. NY217118, NY219024, NY219026), the Natural Science Foundation of the Jiangsu Higher Education Institutions of China (18KJB140009, 19KJB510047), the Fundamental Research Funds for the Central Universities (Grant No.021014380080), the Innovation Research Project of Jiangsu Province (Grant No. CZ007SC19015), High-level Innovation and Entrepreneurship Talents Introduction Program of Jiangsu Province of China. W.Q. Liu acknowledges the financial support from UK EPSRC EP/S010246/1, Royal Society IEC\NSFC\181680, and Leverhulme Trust LTSRF1819\15\12. Y.-W. Fang acknowledges the computational resources provided by the New York University Shanghai and the valuable discussions with Alex Taekyung Lee (Yale University). Diamond Light Source is acknowledged to I10 under proposal SI20748.

References

[1] N. Lu, P. Zhang, Q. Zhang, R. Qiao, Q. He, H. B. Li, Y. Wang, J. Guo, D. Zhang, Z. Duan, Z. Li, M. Wang, S. Yang, M. Yan, E. Arenholz, S. Zhou, W. Yang, L. Gu, C. W. Nan, J. Wu, Y. Tokura, P. Yu, *Nature* **2017**, *546*, 124.

[2] D. Li, K. Lee, B. Y. Wang, M. Osada, S. Crossley, H. R. Lee, Y. Cui, Y. Hikita, H. Y. Hwang, *Nature* **2019**, *572*, 624.

[3] D. C. Vaz, P. Noel, A. Johansson, B. Gobel, F. Y. Bruno, G. Singh, S. McKeown-Walker, F. Trier, L. M. Vicente-Arche, A. Sander, S. Valencia, P. Bruneel, M. Vivek, M. Gabay, N. Bergeal, F. Baumberger, H. Okuno, A. Barthelemy, A. Fert, L. Vila, I. Mertig, J. P. Attane, M. Bibes, *Nat. Mater.* **2019**, *18*, 1187.

[4] D. V. Christensen, F. Trier, W. Niu, Y. Gan, Y. Zhang, T. S. Jespersen, Y. Chen, N. Pryds, *Adv. Mater. Interfaces* **2019**, *6*, 1900772.

[5] A. Ohtomo, H. Y. Hwang, *Nature* **2004**, *427*, 423.

[6] Y. Z. Chen, N. Bovet, F. Trier, D. V. Christensen, F. M. Qu, N. H. Andersen, T. Kasama, W. Zhang, R. Giraud, J. Dufouleur, T. S. Jespersen, J. R. Sun, A. Smith, J. Nygard, L. Lu, B. Buchner, B. G. Shen, S. Linderoth, N. Pryds, *Nat. Commun.* **2013**, *4*, 1371.

[7] H. Zhang, X. Yan, X. Zhang, S. Wang, C. Xiong, H. Zhang, S. Qi, J. Zhang, F. Han, N. Wu, B. G. Liu, Y. Chen, B. Shen, J. Sun, *ACS Nano* **2019**, *13*, 609.

[8] W. Niu, Y. Chen, Y. Gan, Y. Zhang, X. Zhang, X. Yuan, Z. Cao, W. Liu, Y. Xu, R. Zhang, N. Pryds, Y. Chen, Y. Pu, X. Wang, *Appl. Phys. Lett.* **2019**, *115*, 061601.

[9] H. Chen, A. Millis, *Journal of physics. Condensed matter : an Institute of Physics journal* **2017**, *29*, 243001.

[10] Z. Zhong, P. Hansmann, *Phys. Rev. X* **2017**, *7*, 011023.

[11] M. Shen, Y. Weng, Y. Yi, Q. Geng, W. Yan, H. Wang, J. Yang, X. a. Li, *J. Appl. Phys.* **2019**, *126*, 085307.

[12] X. Liu, M. Kotiuga, H. S. Kim, A. T. N'Diaye, Y. Choi, Q. Zhang, Y. Cao, M. Kareev, F. Wen, B. Pal, J. W. Freeland, L. Gu, D. Haskel, P. Shafer, E. Arenholz, K. Haule, D. Vanderbilt, K. M. Rabe, J. Chakhalian, *Proc. Natl. Acad. Sci.* **2019**, *116*, 19863.

[13] X. R. Wang, C. J. Li, W. M. Lü, T. R. Paudel, D. P. Leusink, M. Hoek, N. Poccia, A. Vailionis, T. Venkatesan, J. M. D. Coey, E. Y. Tsymbal, Ariando, H. Hilgenkamp, *Science* **2015**, *349*, 716.

[14] M. Li, C. Tang, T. R. Paudel, D. Song, W. Lu, K. Han, Z. Huang, S. Zeng, X. Renshaw Wang, P. Yang, Ariando, J. Chen, T. Venkatesan, E. Y. Tsymbal, C. Li, S. J. Pennycook, *Adv. Mater.* **2019**, *31*, e1901386.

[15] P. Yu, J. S. Lee, S. Okamoto, M. D. Rossell, M. Huijben, C. H. Yang, Q. He, J. X. Zhang, S. Y. Yang, M. J. Lee, Q. M. Ramasse, R. Erni, Y. H. Chu, D. A. Arena, C. C. Kao, L. W. Martin, R. Ramesh, *Phys. Rev. Lett.* **2010**, *105*, 027201.

[16] L. M. Zheng, X. R. Wang, W. M. Lu, C. J. Li, T. R. Paudel, Z. Q. Liu, Z. Huang, S. W. Zeng, K. Han, Z. H. Chen, X. P. Qiu, M. S. Li, S. Yang, B. Yang, M. F. Chisholm, L. W. Martin, S. J. Pennycook, E. Y. Tsymbal, J. M. D. Coey, W. W. Cao, *Nat. Commun.* **2018**, *9*, 1897.

[17] T. C. Kaspar, P. V. Sushko, S. R. Spurgeon, M. E. Bowden, D. J. Keavney, R. B. Comes, S. Saremi, L. Martin, S. A. Chambers, *Adv. Mater. Interfaces* **2018**, *6*, 1801428.

[18] Z. Chen, Z. Chen, Z. Q. Liu, M. E. Holtz, C. J. Li, X. R. Wang, W. M. Lü, M. Motapothula, L. S. Fan, J. A. Turcaud, L. R. Dedon, C. Frederick, R. J. Xu, R. Gao, A. T. N'Diaye, E. Arenholz, J. A. Mundy, T. Venkatesan, D. A. Muller, L.-W. Wang, J. Liu, L. W. Martin, *Phys. Rev. Lett.* **2017**, *119*, 156801.

[19] J. Zhang, Z. Zhong, X. Guan, X. Shen, J. Zhang, F. Han, H. Zhang, H. Zhang, X. Yan, Q. Zhang, L. Gu, F. Hu, R. Yu, B. Shen, J. Sun, *Nat. Commun.* **2018**, *9*, 1923.

[20] D. Meng, H. Guo, Z. Cui, C. Ma, J. Zhao, J. Lu, H. Xu, Z. Wang, X. Hu, Z. Fu, R.

Peng, J. Guo, X. Zhai, G. J. Brown, R. Knize, Y. Lu, *Proc. Natl. Acad. Sci.* **2018**, *115*, 2873.
[21] G. Araizi-Kanoutas, J. Geessinck, N. Gauquelin, S. Smit, X. H. Verbeek, S. K. Mishra, P. Bencok, C. Schlueter, T.-L. Lee, D. Krishnan, J. Fatermans, J. Verbeeck, G. Rijnders, G. Koster, M. S. Golden, *Phys. Rev. Mater.* **2020**, *4*, 026001.
[22] W. Niu, W. Liu, M. Gu, Y. Chen, X. Zhang, M. Zhang, Y. Chen, J. Wang, J. Du, F. Song, X. Pan, N. Pryds, X. Wang, P. Wang, Y. Xu, Y. Chen, R. Zhang, *Adv. Electron. Mater.* **2018**, *4*, 1800055.
[23] E.-J. Guo, R. Desautels, D. Keavney, M. A. Roldan, B. J. Kirby, D. Lee, Z. Liao, T. Charlton, A. Herklotz, T. Z. Ward, M. R. Fitzsimmons, H. N. Lee, *Sci. Adv.* **2019**, *5*, eaav5050.
[24] D. Fuchs, C. Pinta, T. Schwarz, P. Schweiss, P. Nagel, S. Schuppler, R. Schneider, M. Merz, G. Roth, H. v. Löhneysen, *Phys. Rev. B* **2007**, *75*, 144402.
[25] H. Zhang, J. Zhang, H. Yang, Q. Lan, D. Hong, S. Wang, X. Shen, T. Khan, R. Yu, J. Sun, B. Shen, *ACS Appl. Mater. Interfaces* **2016**, *8*, 18328.
[26] Y. Li, S. J. Peng, D. J. Wang, K. M. Wu, S. H. Wang, *AIP AdV.* **2018**, *8*, 056317.
[27] E.-J. Guo, R. D. Desautels, D. Keavney, A. Herklotz, T. Z. Ward, M. R. Fitzsimmons, H. N. Lee, *Phys. Rev. Mater.* **2019**, *3*, 014407.
[28] V. V. Mehta, N. Biskup, C. Jenkins, E. Arenholz, M. Varela, Y. Suzuki, *Phys. Rev. B* **2015**, *91*, 144418.
[29] N. Biškup, J. Salafranca, V. Mehta, M. P. Oxley, Y. Suzuki, S. J. Pennycook, S. T. Pantelides, M. Varela, *Phys. Rev. Lett.* **2014**, *112*, 087202.
[30] J. W. Freeland, J. X. Ma, J. Shi, *Appl. Phys. Lett.* **2008**, *93*, 212501.
[31] W. S. Choi, J. H. Kwon, H. Jeen, J. E. Hamann-Borrero, A. Radi, S. Macke, R. Sutarto, F. He, G. A. Sawatzky, V. Hinkov, M. Kim, H. N. Lee, *Nano Lett* **2012**, *12*, 4966.
[32] A. D. Rata, A. Herklotz, L. Schultz, K. Dörr, *Eur. Phys. J. B* **2010**, *76*, 215.
[33] W. Liu, Y. Xu, L. He, G. v. d. Laan, R. Zhang, K. Wang, *Sci. Adv.* **2019**, *5*, eaav2088.
[34] M. Merz, P. Nagel, C. Pinta, A. Samartsev, H. v. Löhneysen, M. Wissinger, S. Uebe, A. Assmann, D. Fuchs, S. Schuppler, *Phys. Rev. B* **2010**, *82*, 174416.
[35] A. Herklotz, A. D. Rata, L. Schultz, K. Dörr, *Phys. Rev. B* **2009**, *79*, 092409.
[36] J. E. Hamann-Borrero, S. Macke, W. S. Choi, R. Sutarto, F. He, A. Radi, I. Elfimov, R. J. Green, M. W. Haverkort, V. B. Zabolotnyy, H. N. Lee, G. A. Sawatzky, V. Hinkov, *npj Quantum Mater.* **2016**, *1*, 16013.
[37] S. Li, J. Wang, Q. Zhang, M. A. Roldan, L. Shan, Q. Jin, S. Chen, Z. Wu, C. Wang, C. Ge, M. He, H. Guo, L. Gu, K.-j. Jin, E.-J. Guo, *Phys. Rev. Mater.* **2019**, *3*, 114409.
[38] C. F. Chang, Z. Hu, H. Wu, T. Burnus, N. Hollmann, M. Benomar, T. Lorenz, A. Tanaka, H. J. Lin, H. H. Hsieh, C. T. Chen, L. H. Tjeng, *Phys Rev Lett* **2009**, *102*, 116401.
[39] J. H. Jang, Y. M. Kim, Q. He, R. Mishra, L. Qiao, M. D. Biegalski, A. R. Lupini, S. T. Pantelides, S. J. Pennycook, S. V. Kalinin, A. Y. Borisevich, *ACS Nano* **2017**, *11*, 6942.
[40] P. M. Raccah, J. B. Goodenough, *Phys. Rev.* **1967**, *155*, 932.
[41] Y. Chen, R. J. Green, R. Sutarto, F. He, S. Linderoth, G. A. Sawatzky, N. Pryds, *Nano. Lett.* **2017**, *17*, 7062.
[42] M. Nord, P. E. Vullum, M. Moreau, J. E. Boschker, S. M. Selbach, R. Holmestad, T. Tybell, *Appl. Phys. Lett.* **2015**, *106*, 041604.
[43] S. Lee, A. T. Lee, A. B. Georgescu, G. Fabbris, M.-G. Han, Y. Zhu, J. W. Freeland, A. S. Disa, Y. Jia, M. P. M. Dean, F. J. Walker, S. Ismail-Beigi, C. H. Ahn, *Phys. Rev. Lett.* **2019**, *123*, 117201.
[44] J. S. Lee, Y. W. Xie, H. K. Sato, C. Bell, Y. Hikita, H. Y. Hwang, C. C. Kao, *Nat. Mater.* **2013**, *12*, 703.
[45] J. Biscaras, N. Bergeal, S. Hurand, C. Grossetete, A. Rastogi, R. C. Budhani, D. LeBoeuf, C. Proust, J. Lesueur, *Phys. Rev. Lett.* **2012**, *108*, 247004.
[46] J. Garcia-Barriocanal, J. C. Cezar, F. Y. Bruno, P. Thakur, N. B. Brookes, C. Utfeld, A. Rivera-Calzada, S. R. Giblin, J. W. Taylor, J. A. Duffy, S. B. Dugdale, T. Nakamura, K.

Kodama, C. Leon, S. Okamoto, J. Santamaria, *Nat. Commun.* **2010**, *1*, 82.
[47] J. R. L. Mardegan, D. V. Christensen, Y. Z. Chen, S. Parchenko, S. R. V. Avula, N. Ortiz-Hernandez, M. Decker, C. Piamonteze, N. Pryds, U. Staub, *Phys. Rev. B* **2019**, *99*, 134423.
[48] Y. Z. Chen, F. Trier, T. Wijnands, R. J. Green, N. Gauquelin, R. Egoavil, D. V. Christensen, G. Koster, M. Huijben, N. Bovet, S. Macke, F. He, R. Sutarto, N. H. Andersen, J. A. Sulpizio, M. Honig, G. E. Prawiroatmodjo, T. S. Jespersen, S. Linderoth, S. Ilani, J. Verbeeck, G. Van Tendeloo, G. Rijnders, G. A. Sawatzky, N. Pryds, *Nat. Mater.* **2015**, *14*, 801.
[49] A. Chainani, M. Mathew, D. D. Sarma, *Phys. Rev. B* **1992**, *46*, 9976.
[50] P. W. Tasker, *J. Phys. C: Solid State Phys.* **1979**, *12*, 4977.
[51] J. Lee, A. A. Demkov, *Phys. Rev. B* **2008**, *78*, 193104.
[52] E. Dagotto, T. Hotta, A. Moreo, *Phys. Rep.* **2001**, *344*, 1.
[53] Ariando, X. Wang, G. Baskaran, Z. Q. Liu, J. Huijben, J. B. Yi, A. Annadi, A. R. Barman, A. Rusydi, S. Dhar, Y. P. Feng, J. Ding, H. Hilgenkamp, T. Venkatesan, *Nat. Commun.* **2011**, *2*, 188.
[54] S. Stemmer, A. J. Millis, *MRS Bulletin* **2013**, *38*, 1032.
[55] Y. Chen, N. Pryds, J. E. Kleibeuker, G. Koster, J. Sun, E. Stamate, B. Shen, G. Rijnders, S. Linderoth, *Nano Lett.* **2011**, *11*, 3774.
[56] Y. Hotta, T. Susaki, H. Y. Hwang, *Phys. Rev. Lett.* **2007**, *99*, 236805.
[57] S. A. Chambers, L. Qiao, T. C. Droubay, T. C. Kaspar, B. W. Arey, P. V. Sushko, *Phys. Rev. Lett.* **2011**, *107*, 206802.
[58] P. Xu, W. Han, P. M. Rice, J. Jeong, M. G. Samant, K. Mohseni, H. L. Meyerheim, S. Ostanin, I. V. Maznichenko, I. Mertig, E. K. Gross, A. Ernst, S. S. Parkin, *Adv. Mater.* **2017**, *29*, 1604447.
[59] M. N. Grisolia, J. Varignon, G. Sanchez-Santolino, A. Arora, S. Valencia, M. Varela, R. Abrudan, E. Weschke, E. Schierle, J. E. Rault, J. P. Rueff, A. Barthelemy, J. Santamaria, M. Bibes, *Nat Phys* **2016**, *12*, 484.
[60] G. Kresse, J. Furthmüller, *Comp. Mater. Sci.* **1996**, *6*, 15.
[61] G. Kresse, J. Furthmuller, *Phys. Rev. B* **1996**, *54*, 11169.
[62] J. P. Perdew, A. Ruzsinszky, G. I. Csonka, O. A. Vydrov, G. E. Scuseria, L. A. Constantin, X. Zhou, K. Burke, *Phys Rev Lett* **2008**, *100*, 136406.

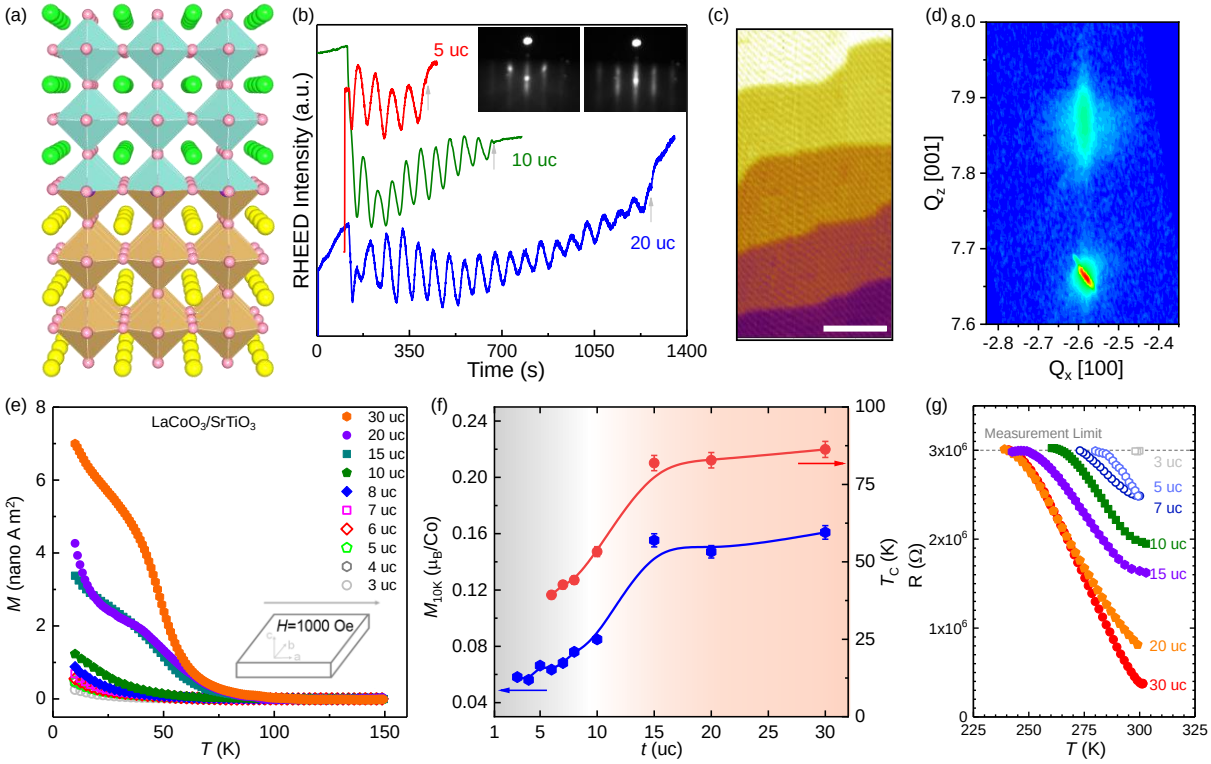

Figure 1. Epitaxial growth and characterizations of LCO/STO heterostructures. a) Sketch of the LCO/STO heterostructures. b) Typical RHEED oscillations of LCO/STO heterostructures. The insets from left to right are the RHEED patterns before and after deposition of the 20-uc LCO, respectively. c) Surface morphology of a typical 20 uc-LCO/STO heterostructure. The scale bar is 400 nm. d) RSM of an LCO/STO heterostructure with a thickness of 60 uc. Note that the film is fully strained on the substrate without any release, at least up to a thickness of 60 uc (~ 24 nm). e) Temperature-dependent magnetic moments of heterostructures with the thickness of LCO ranging from 3 to 30 uc. The magnetization measurement configuration is shown in the inset. f) Thickness dependence of the magnetic moments at 10 K and *T*c of LCO/STO heterostructures. g) Temperature dependent sheet resistance of LCO/STO heterostructures with various thickness.

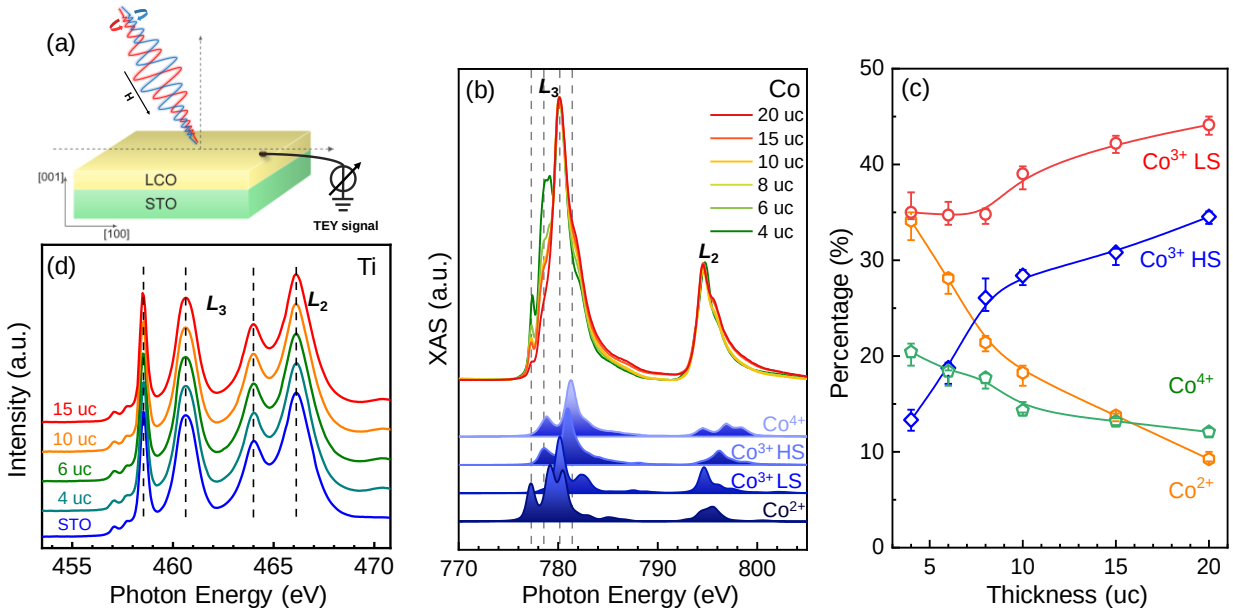

Figure 2. Multivalent states of Co in LCO/STO heterostructures. a) The schematic diagram of the experimental configuration for the XAS/XMCD measurements. b) Normalized isotropic XAS spectra at Co-$L_{2,3}$ edges of LCO/STO heterostructures together with reference spectra for various valent Co ions. Grey dashed lines are guidelines for peak positions with different valent states. c) Different concentration of various Co ion states deconvoluted from the XAS spectra. d) Ti-$L_{2,3}$ edge XAS spectra of LCO/STO heterostructures and bare STO substrate. All spectra were obtained at 10 K in TEY model.

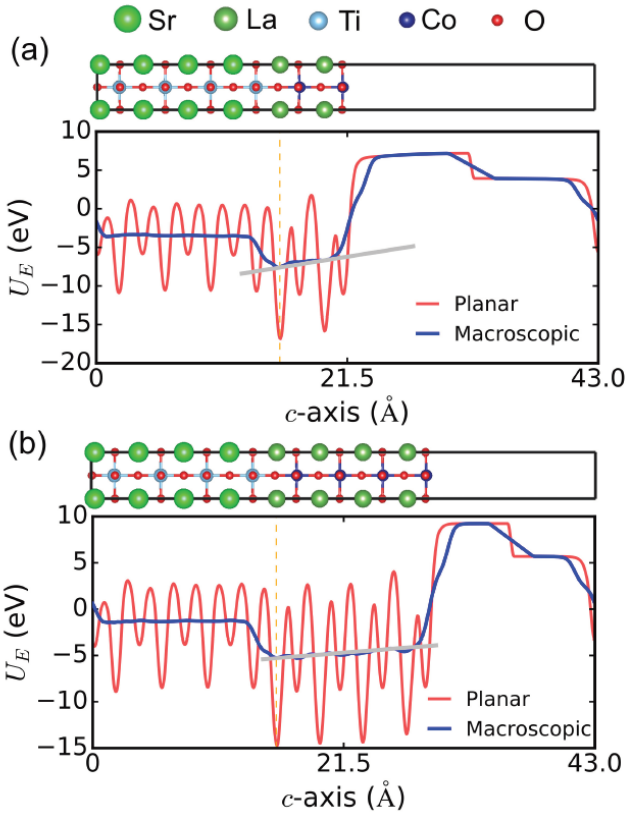

Figure 3. The structures and potential energy profiles U_E for a) $(LCO)_2/(STO)_4$ and b) $(LCO)_4/(STO)_4$. In the panels of potential energy profiles, the *ab* planar-averaged and the macroscopic-averaged potential energy are shown by the red and blue lines, respectively. The dashed orange lines refer to the LaO layer adjacent to the STO substrate. The slope of the silver lines corresponds to the internal electric fields.

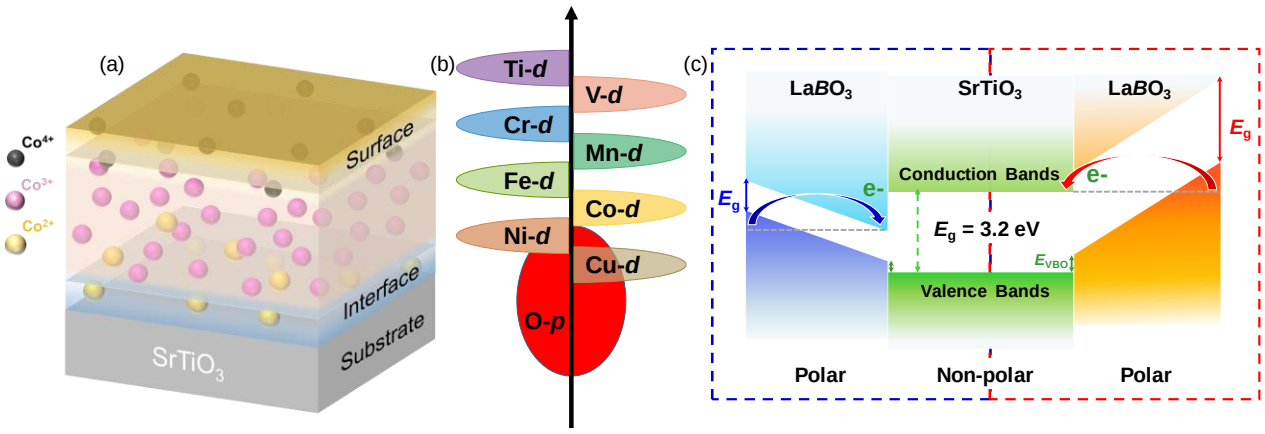

Figure 4. Charge transfer of the La*B*O$_3$/SrTiO$_3$ heterostructures and resultant properties. a) Multivalent states of Co ions distribute in the LCO/STO heterostructures. b) Energy level of transition metal 3*d* states verse oxygen 2*p* states in the La*B*O$_3$/SrTiO$_3$ heterostructures (*B*= Ti, V, Cr, Mn, Fe, Co, Ni and Cu). c) Schematic band diagram of La*B*O$_3$/SrTiO$_3$ interface for charge transfer.